Powered by Rust™

J.W. Long, M.B. Sassin, and D.R. Rolison
Chemistry Division

Making Rust Useful: The cost, country of origin, and environmental impact of state-of-the-art materials that store energy in batteries and electrochemical capacitors (ECs) propel the ongoing search for charge-storage materials beyond the oxides of nickel, cobalt, or ruthenium. By applying the design concept of "multifunctional electrode nanoarchitectures," pioneered by NRL's Advanced Electrochemical Materials Section,[1] we transform an otherwise uninteresting battery material, iron oxide (FeOx) — also known as rust — into a battery- and EC-relevant form in which the oxide is painted as a nanometers-thick coating on the walls of a sponge-like, conductive scaffold.

The Right Kind of Electrode Architecture: To incorporate FeOx as nanoscale rust into electrode nanoarchitectures, we have developed a low-cost, solution-based deposition process predicated on the redox reaction between aqueous potassium ferrate (K$_2$FeO$_4$, a strong oxidant) and the electron-rich surfaces of ultraporous carbon-based scaffolds (Fig. 1, top).[2] Our scaffold of choice is carbon-fiber-paper-supported carbon nanofoam, which offers us an ideal platform to design high-performance electrode architectures with such inherent and important attributes as high specific surface area (300–500 m^2 g^{-1}), high electrical conductivity (20–40 S cm^{-1}), through-connected networks of size-tunable pores (nanometers to micrometers), and synthetic scalability in length and width (~100 cm^2) as well as thickness (70–300 μm).

These device-ready carbon substrates have macroscale form factors that present challenges to achieving homogeneous coatings because the internal surfaces are non-line-of-sight and accessed by tortuous and size-disperse pore networks. We identified solution conditions to self-limit the reaction of ferrate at carbon, resulting in conformal deposits of FeOx nanoribbons (10–20 nm thick) that permeate the macroscopic thickness of the nanofoam substrate (up to 150 μm), while leaving the 3D plumbing of the carbon nanofoam intact (Fig. 1, bottom center).[2] The direct reaction of the ferrate precursor and carbon surface also ensures intimate physical and electrical association between the FeOx and the underlying carbon nanoarchitecture (Fig. 1, bottom right), which ultimately supports electrochemical performance and stability under challenging operating conditions. Characterization of the resulting materials by X-ray absorption spectroscopy confirms that the form of iron oxide produced by the ferrate–carbon reaction is a hydrated Fe(III)-oxide and a close relative of rust.

Enhanced Power with Well-Wired Rust: Bulk forms of FeOx perform poorly as electrode materials because of modest electronic and ionic conductivity, but when distributed as a nanoscale coating on a 3D conductor, such as carbon nanofoam, FeOx exhibits
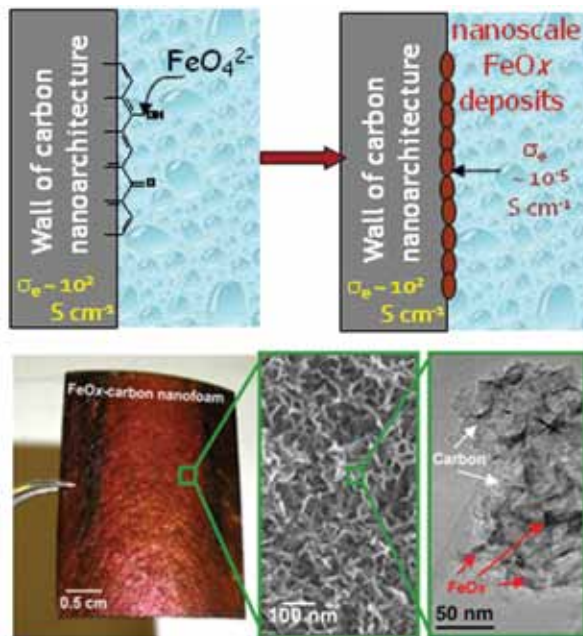

FIGURE 1
Schematic of FeOx deposition process (top); optical image (bottom left), scanning electron micrograph (bottom center), and transmission electron micrograph (bottom right) of an FeOx−carbon nanofoam.

high charge-storage capacity and rapid charge–discharge characteristics. Preliminary electrochemical measurements in mild aqueous electrolytes (e.g., 2.5 M Li$_2$SO$_4$) demonstrate that the addition of the FeOx coating, even at modest oxide mass loadings (~30 wt %), significantly increases the total mass- (3×), volume- (7×), and area-normalized (7×) capacitance of the carbon nanofoam (Fig. 2). The larger enhancement in the volume- and area-normalized capacitance results from the multifunctional electrode architecture design, because painting the walls of the nanofoam with FeOx does not increase the volume or geometric footprint of the electrode. The additional capacitance provided by the rust paint (~340 F per gram of FeOx) is due to the reversible electrochemical toggling of the Fe oxidation state between 3.0 and 2.7 (Fig. 2) and is threefold higher than previously reported for iron oxides tested under similar electrochemical conditions.[2] By designing the electrode as a multifunctional architecture we maximize the charge-storage utilization of the FeOx coating, while also projecting the ultrathin coating in three dimensions to achieve technologically relevant footprint-normalized metrics (2D: mF cm^{-2} vs 3D: F cm^{-2}).
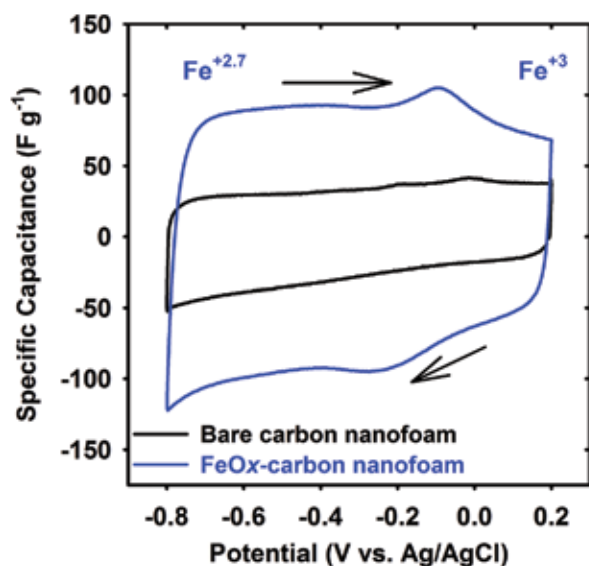
FIGURE 2
Specific capacitance vs potential for bare carbon nanofoam (black curve) and an FeOx–carbon nanofoam (blue curve) in 2.5 M Li_2SO_4 at 5 mV s^{-1}.

Devices and Batteries: Prototype asymmetric EC devices with FeOx–carbon as the negative electrode and analogously designed MnOx–carbon[3] as the positive electrode sustain operating cell voltages of ~2 V in mild aqueous electrolytes. The increased operating voltage beyond the thermodynamic window of H_2O (~1.2 V) is due to the poor hydrogen-evolution kinetics at the FeOx negative electrode (Fig. 3). Adding the extra energy of a wider voltage window to the enhanced charge-storage capabilities of the metal oxide–painted carbon nanofoams results in cell-level specific capacitances of >30 F g^{-1} and an energy density of 13.5 W h kg^{-1}; ECs composed of powder-composite electrode structures of MnOx and FeOx deliver only 7 W h kg^{-1}. The energy density of the EC prototype MnOx(+) || FeOx(−) can be extracted within tens of seconds, revealing that the multifunctional electrode architecture enables enhancements in capacity and energy density while maintaining the high-rate capabilities characteristic of the underlying carbon nanofoam substrate. More recently, we demonstrated that the applications of these rust-painted structures extend beyond ECs to serve as high-performance anode materials for Li-ion batteries.

Summary: Next-generation ECs and batteries that incorporate these advanced electrode structures should bridge the current performance gap between the high energy density of batteries and the high power density of ECs. We can now design power sources that deliver energy over mission-relevant time scales as well as deliver on-demand burst-power in a single device.
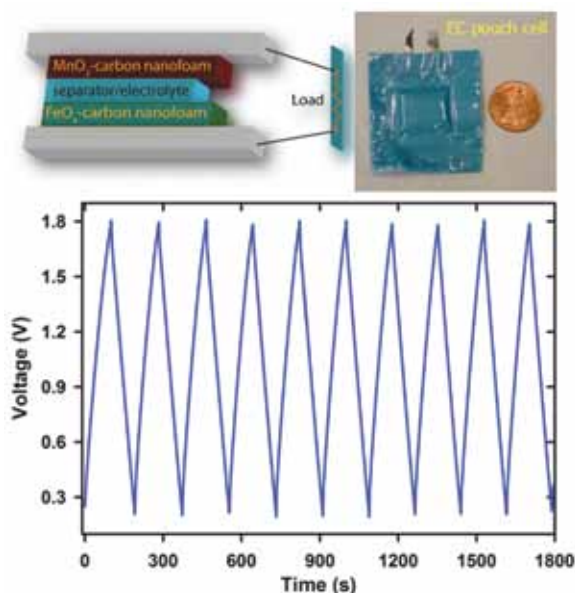

FIGURE 3
Schematic of an aqueous asymmetric EC cell with a MnOx–carbon nanofoam positive electrode and an FeOx–carbon nanofoam negative electrode (top left); optical image of prototype MnOx(+) || FeOx(−) EC cell (top right); galvanostatic charge–discharge curves of a MnOx(+) || FeOx(−) EC pouch cell between 0.2 and 1.8 V (bottom).

This next generation of energy-storage devices will support such critical military and consumer applications as telecommunications, bridge/backup power, and hybrid-electric vehicles.

[Sponsored by ONR]

References
[1] D.R. Rolison, J.W. Long, J.C. Lytle, A.E. Fischer, C.P. Rhodes, M.E. Bourg, and A.M. Lubers, "Multifunctional 3D Nanoarchitectures for Energy Storage and Conversion," *Chem. Soc. Rev.* **38**, 226–252 (2009).
[2] M.B. Sassin, A.N. Mansour, K.A. Pettigrew, D.R. Rolison, and J.W. Long, "Electroless Deposition of Conformal Nanoscale Iron Oxide on Carbon Nanoarchitectures for Electrochemical Charge Storage," *ACS Nano* **4**, 4505–4514 (2010).
[3] A.E. Fischer, K.A. Pettigrew, D.R. Rolison, and J.W. Long, "Incorporation of Homogeneous, Nanoscale MnO$_2$ within Ultraporous Carbon Structures via Self-Limiting Electroless Deposition: Implications for Electrochemical Capacitors," *Nano Lett.* **7**, 281–286 (2007). ∎

Anomalously Large Linear Magnetoresistance Effects in Graphene

A.L. Friedman[1] and P.M. Campbell[2]
[1]*National Research Council Postdoctoral Associate*
[2]*Electronics Science and Technology Division*

Introduction: In the 1960s, it was discovered that interesting galvanometric behavior could result from the

addition of small inhomogeneities in device materials.[1] Specifically, Abrikosov developed a model for quantum linear magnetoresistance (LMR) in which a system confined to the "extreme quantum limit" at low temperature as a result of inhomogeneities that are small compared to the device size will exhibit a large, non-saturating LMR as opposed to the usual quadratic and then low-field saturating magnetoresistance (MR) of most conductors.[2] However, LMR is only now garnering attention because of the recent discovery of several narrow bandgap semiconductors with the high mobilities required of the Abrikosov model. Recent research has shown that there are classical analogues to quantum LMR.[3] By incorporating highly conductive impurities in devices in the form of metallic shunts,[4] these classical models predict that an even larger linear MR (called extraordinary magnetoresistance, or EMR) can be achieved. Graphene is a hexagonally ordered monolayer of carbon atoms that, due to its zero bandgap, high room-temperature mobility, and zero effective mass, provides the perfect platform for the realization of room-temperature LMR and EMR devices. These devices show much promise for future use as magnetic sensors and in memory device applications.

Quantum Linear Magnetoresistance: Despite predictions, LMR has yet to be observed in graphene devices because the large-amplitude Shubnikov–de Haas oscillations (SdHO) and quantum Hall effect observed in clean, homogeneous exfoliated graphene (the current experimental standard) overwhelm and obscure any linear dependence. However, epitaxially grown multilayer graphene devices on the carbon face of SiC can allow LMR observation because of their disorder. Raman spectroscopy (Fig. 4(d)) finds two types of inhomogeneity in the devices: (1) a variation of film thickness across the device with an average of 16 ± 3 nm and (2) a graphene grain size of ~1.5 µm, which is much smaller than the device length (~125 µm). Despite these inhomogeneities, research has shown that in multilayer epitaxially grown graphene, layers are essentially noninteracting and conduction properties are similar to those of single-monolayer graphene. Figure 4(a) shows quantum LMR from 2.2 K
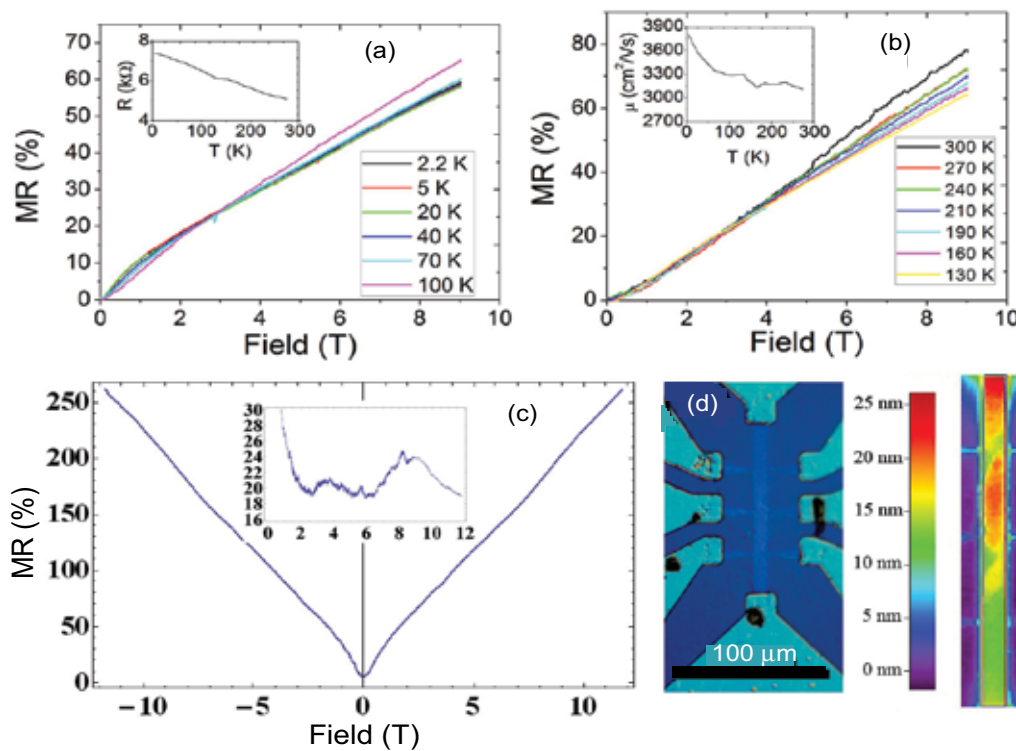

FIGURE 4

(a) Quantum LMR from 2.2 K to 100 K. The inset shows the resistance as a function of temperature. (b) Quantum LMR from 130 K to 300 K. The inset shows the mobility as a function of temperature. (c) Large MR value (250% at 12 T) obtained from a quantum LMR sample at 4.2 K. The inset shows the Shubnikov–de Haas oscillations at 4.2 K. (d) Nomarski image (left) showing the LMR device and corresponding Raman spectroscopy map (right) indicating inhomogeneities in the device necessary for the unmasking of the LMR behavior.
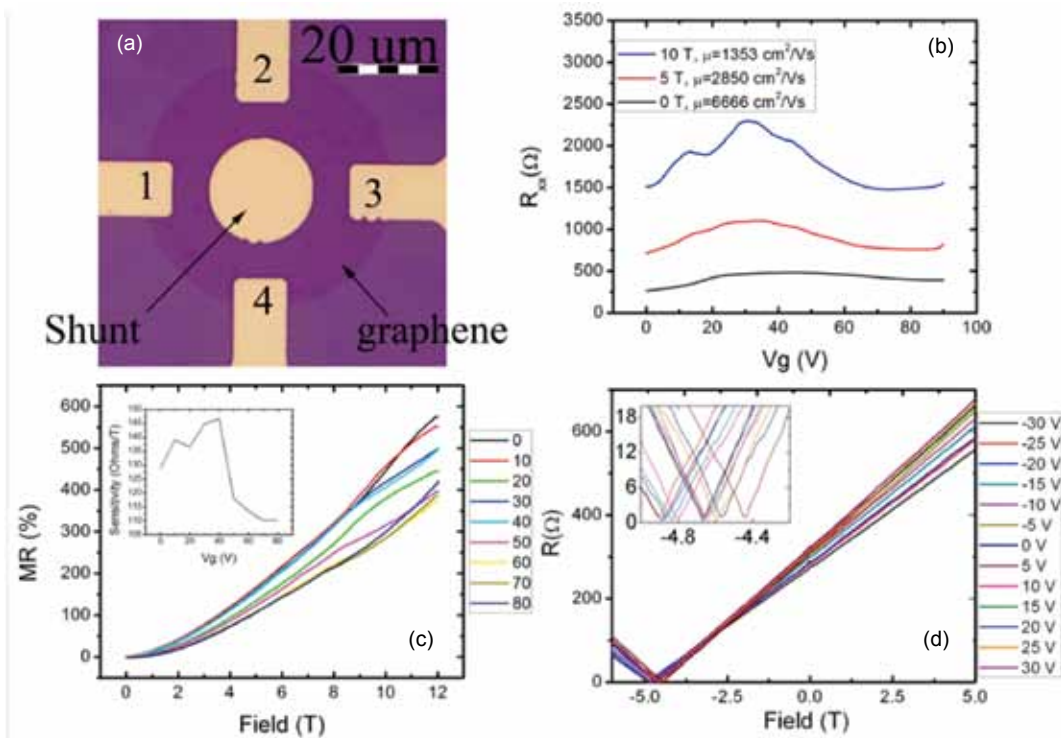
FIGURE 5
(a) Shunted graphene van der Pauw disk device. (b) Resistance vs gate voltage for several applied magnetic fields. (c) MR vs field for a variety of gate voltages. The inset shows the sensitivity as a function of gate voltage, which corresponds to the Dirac point. (d) Resistance vs field at a variety of gate voltages for the device operated in the Hall measurement configuration.

to 100 K. The behavior of the device changes very little over this temperature range. Figure 4(b) shows quantum LMR from 130 K to 300 K. To date, this is the only reported observation of room temperature quantum LMR. The insets of Figs. 4(a) and (b) show the resistance and the mobility, respectively, of the device as a function of temperature. It is precisely because of the small change in resistance and mobility as the temperature increases, along with graphene's zero effective mass, that the conditions for quantum LMR are satisfied even at room temperature. Figure 4(c) shows quantum LMR at 4.2 K in a sample in which the MR reached ~250% at 12 T. The small SdHO shown in the inset of Fig. 4(c) were extracted from the data and further attest to the quantum nature of the effect.

Extraordinary Magnetoresistance: Figure 5(a) shows an optical image of a shunted graphene device grown by chemical vapor deposition. Based on the calculated components of the conductivity tensor, in zero magnetic field, the current will flow through the shunt, while in a magnetic field, the current will tend to flow around the shunt and redistribute in the graphene film. The larger the magnetic field, the more current

flows through the graphene and not the shunt. This translates to an enhancement in the MR. EMR devices exploit geometric changes in devices to maximize MR signal. Therefore, the MR can be further maximized by changing the size of the shunt and the contact measurement configuration. Figure 5(b) shows a graph of resistance vs gate voltage at different magnetic fields. At zero field, the curve is relatively featureless. The mobility is very high as most of the current flows through the shunt. As the field increases, a Dirac point becomes evident and the mobility decreases, eventually to saturate at the mobility of the graphene film, as more current flows around the shunt and redistributes in the graphene. Hall oscillations become visible at 10 T. Figure 5(c) shows the MR of the device with the current (10 μA) passed between electrodes 1 and 4, and voltage measured between electrodes 2 and 3 at 4.2 K. The measured MR of ~600% at 12 T is the highest MR measured thus far in graphene. The inset of Fig. 5(c) shows the sensitivity of the device, which corresponds to the Dirac point. Figure 5(d) shows resistance measured in the Hall configuration (current passed between electrodes 1 and 3 and voltage measured between electrodes 2 and 4). The devices show a gate-tunable

minimum in MR instead of the usual zero MR at zero field, which is most likely caused by chemical dopants remaining from processing that are trapped beneath the shunt. This suggests that with controlled chemical doping, we can choose the position of this minimum and can exploit it for device purposes.

Conclusions: As the search for applications for graphene continues — particularly applications that do not require a bandgap or atomic-scale chemical modification — devices that make simple use of graphene's innate properties will become more important. The large, linear MR in both LMR and EMR can be used in a variety of applications including read-heads and magnetic sensors. Graphene is also easily scalable without compromising any of its inherent characteristics, which is an important difference over the narrow-gap semiconductors currently used in EMR device applications. We measure a signal-to-noise ratio of ~30 dB at 1 GHz and 50 mT, which makes these devices slightly better than similar devices made of narrow-gap semiconductors. With further optimization of materials and device design, these devices will likely offer sensitivities significantly better than the current state of the art.

[Sponsored by NRL]

References

[1] C. Herring, "Effect of Random Inhomogeneities on Electrical and Galvanomagnetic Measurements," *Journal of Applied Physics* **31**, 1939–1953 (1960).

[2] A. Abrikosov, "Galvanometric Phenomena in Metals in the Quantum Limit," *Sov. Phys. JTEP* **29**, 746 (1969).

[3] M.M. Parish and P.B. Littlewood, "Non-Saturating Magnetoresistance in Heavily Disordered Semiconductors," *Nature* **426**, 162–165 (2003).

[4] S.A. Solin, Tineke Thio, D.R. Hines, and J.J. Heremans, "Enhanced Room-Temperature Geometric Magnetoresistance in Inhomogeneous Narrow-Gap Semiconductors," *Science* **289**, 1530–1532 (2000).

■